PCCP

Physical Chemistry Chemical Physics

ROYAL SOCIETY
OF CHEMISTRY
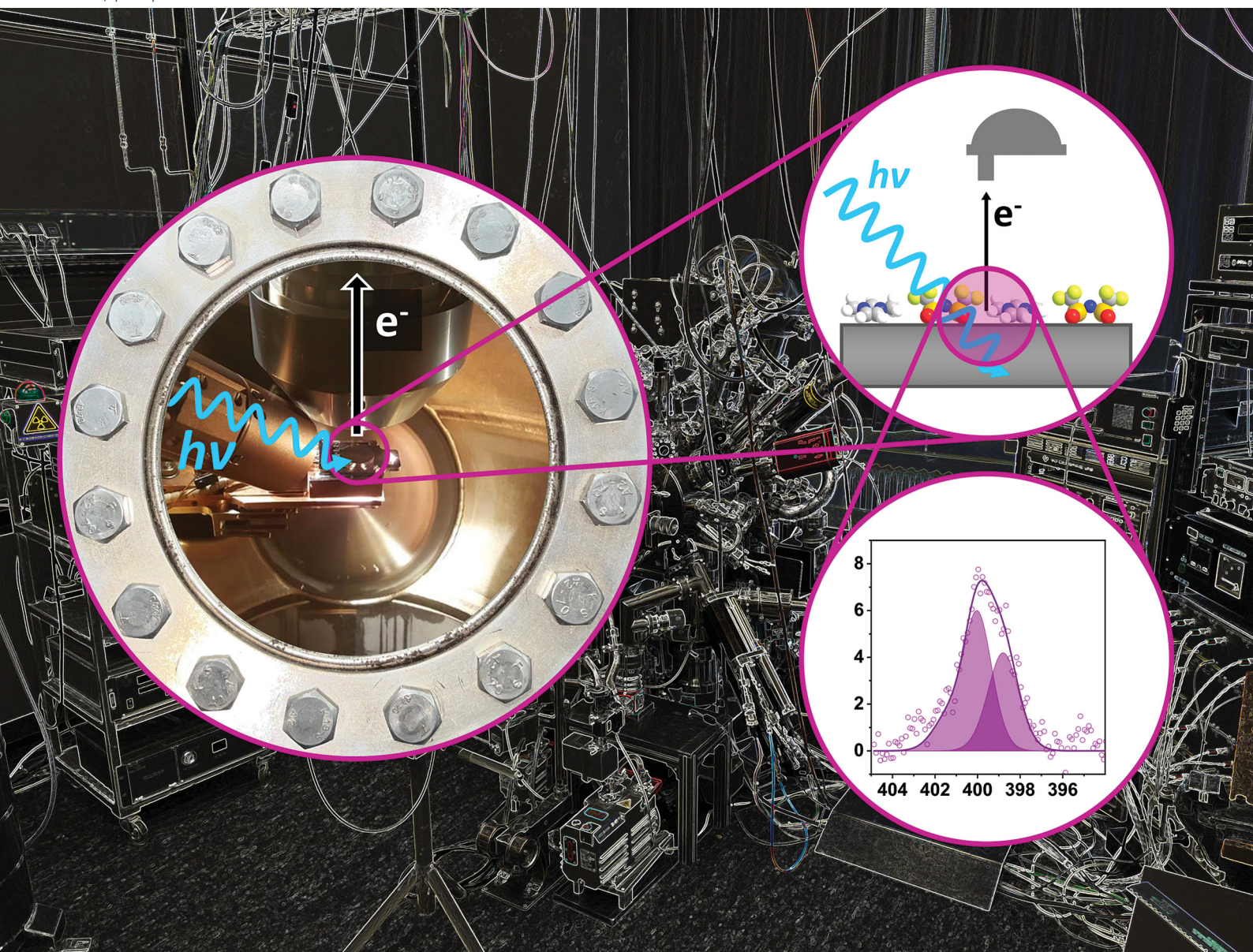
PAPER
Hans-Peter Steinrück *et al.*
Adsorption and thermal evolution of [C$_1$C$_1$Im][Tf$_2$N] on Pt(111)

PCCP
Owner Societies

Check for updates

Adsorption and thermal evolution of [C$_1$C$_1$Im][Tf$_2$N] on Pt(111)†

Stephen Massicot, [ID] Afra Gezmis, [ID] Timo Talwar, [ID] Manuel Meusel, [ID] Simon Jaekel, [ID] Rajan Adhikari, [ID] Leonhard Winter, [ID] Cynthia C. Fernández, [ID] Andreas Bayer, [ID] Florian Maier [ID] and Hans-Peter Steinrück [ID] *

In the context of ionic liquid (IL)-assisted catalysis, we have investigated the adsorption and thermal evolution of the IL 1,3-dimethylimidazolium bis(trifluoromethylsulfonyl)imide ([C$_1$C$_1$Im][Tf$_2$N]) on Pt(111) between 100 and 800 K by angle-resolved X-ray photoelectron spectroscopy and scanning tunneling microscopy. Defined amounts of IL in the coverage range of a complete first wetting layer were deposited at low temperature (100–200 K), and subsequently heated to 300 K, or directly at 300 K. At 100 K, the IL adsorbs as an intact disordered layer. Upon heating to 200 K, the IL stays intact, but forms an ordered and well-oriented structure. Upon heating to 250 K, the surface order increases, but at the same time STM and XPS indicate the onset of decomposition. Upon heating to 300 K, decomposition progresses, such that 50–60% of the IL is decomposed. The anion-related reaction products desorb instantaneously, and the cation-related products remain on the surface. Thereby, the surface is partly passivated, enabling the remaining IL to still be adsorbed intact at 300 K. For IL deposition directly at 300 K, a fraction of the IL instantaneously decomposes, with the anion-related products desorbing, opening free space for further deposition of IL. Hence, cation-related species accumulate at the expense of anions, until one fully closed wetting layer is formed. As a consequence, a higher dose is required to reach this coverage at 300 K, compared to 100–200 K.

Introduction

Catalytic processes in modern industry are in some way involved in the processing of over 80% of all manufactured products.[1] Particularly in the chemical industry, catalysts are even used for the production of about 90% of all chemicals.[2] Pushing towards a more sustainable chemical industry, "greener" and more efficient catalyst technologies have to be developed. In this context, ionic liquids (ILs) have been applied in industrial processes on the large scale.[3–5] ILs are a class of compounds that consist solely of cations and anions and exhibit melting points typically well below 100 °C. Novel catalytic concepts based on ILs were developed like the SCILL (solid catalyst with ionic liquid layer) approach.[6–9] In SCILL, a thin IL film is added to a solid catalyst material – often metal nanoparticles dispersed on a porous support. In the course of the catalytic turnover, the reactants have to pass through the IL layer in order to reach the active sites of the solid catalyst,

where the actual chemical conversion takes place. By exploiting differences in the solubility and diffusion rate of competing reactants (and products), the concentration and reactivity close to the active metal sites can be tuned. More importantly, the IL also interacts directly with the solid catalyst.[10–13] Hereby, the IL can modify sites by ligand-like interactions or block less selective sites of the solid catalyst and thus increase the selectivity of the catalytic process. Such SCILL systems are already commercially available by Clariant for the selective hydrogenation of unsaturated hydrocarbons.[14] In 2017, the Dow Chemical Company started up a new world-scale production site using a SCILL catalyst for the ultra-selective hydrogenation of acetylene to form ethylene, which is a crucial feedstock for the production of a variety of polymers.[15]

Despite successful applications of ILs in the chemical industry, a thorough understanding of SCILL catalysts on the molecular scale is still lacking, particularly with respect to the interface formed between the IL and the solid catalyst, which plays a crucial role as the chemical conversion happens there. Thus, fundamental knowledge about the film growth, wetting, thermal behavior and orientation of the ions at this interface is crucial for SCILL catalysis. These properties can be addressed by detailed surface science studies of thin IL films on metallic substrates as model catalysts. However, mostly less reactive surfaces, like Au(111) or Ag(111), have been investigated so

Lehrstuhl für Physikalische Chemie II, Friedrich-Alexander-Universität Erlangen-Nürnberg, Egerlandstraße 3, 91058 Erlangen, Germany.
E-mail: hans-peter.steinrueck@fau.de

† Electronic supplementary information (ESI) available. See DOI: https://doi.org/10.1039/d3cp02743k

This journal is © the Owner Societies 2023

Phys. Chem. Chem. Phys., 2023, **25**, 27953–27966 | 27953

far,[16–20] and only a few studies exist on more reactive surfaces such as Cu(111),[21,22] Ni(111),[23] Pd(111)[24,25] or Pt(111).[26,27] The latter is particularly interesting since ILs were reported to promote platinum-based fuel cell catalysts,[28] particularly by improving the oxygen reduction reaction.[29,30]

With this work, we aim to thoroughly investigate a more application-relevant IL/metal model system. We chose the IL 1,3-dimethylimidazolium bis(trifluoromethylsulfonyl)imide ([C_1C_1Im][Tf_2N], see top of Fig. 1) since this IL was already well characterized in surface science studies on Au(111), Ag(111) and Cu(111) in our group.[20,21,23,31–35] As model catalyst, we selected the Pt(111) single crystal surface, as platinum-based catalysts are widely used in the chemical industry. Moreover, evaporated IL films of the very similar IL [C_2C_1Im][Tf_2N] on Pt(111) had already been studied by means of infrared spectroscopy.[26,27] We will compare our results to this study, and provide additional insights also for this system. For our model catalytic approach, we used *in situ* physical vapor deposition (PVD) to prepare ultra-thin films of [C_1C_1Im][Tf_2N] on Pt(111). These films were then studied by scanning tunneling microscopy (STM) and angle-resolved X-ray photoelectron spectroscopy (ARXPS).

Experimental

The ionic liquid [C_1C_1Im][Tf_2N] was either bought from IoLiTec (used in the XPS measurements) or synthesized under ultra-clean conditions described in a previous publication (used in the STM measurements).[36] The cation [C_1C_1Im]$^+$ is also known as [MMIm]$^+$ in literature,[37] and the anion [Tf_2N]$^-$ as [NTf$_2$]$^{-38}$ or [TFSA]$^{-}$.[39] The IL was thoroughly degassed under ultra-high vacuum (UHV) prior to deposition to remove volatile impurities. The STM and the ARXPS experiments were performed in two independent UHV systems with base pressures below 2×10^{-10} mbar. Using a home-built Knudsen cell, the IL was deposited onto the Pt(111) crystal at different temperatures by physical vapor deposition (PVD),[40] with the crucible temperature between 385–398 K. It has been shown before that this IL can be evaporated intact.[16] IL coverages are denoted in ML, where 1 ML corresponds to a complete layer of vertically oriented ion pairs with an ion density as in the bulk. For a complete first wetting layer in a checkerboard-like arrangement with anions and cations adsorbing next to each other in direct contact to the surface, this coverage corresponds to 0.5 ML. One should note that the real IL coverage required to form a closed wetting layer at the metal surface can deviate from this 0.5 ML value due to the specific ion/substrate interactions, the resulting adsorption geometry and long-range ordered structures.

All STM measurements were performed using a Scienta Omicron VT-AFM-Q + -XA microscope in a two-chamber UHV system. The Pt(111) surface was cleaned by Ar$^+$ ion sputtering (1 keV), annealing at 1100 K for 10 min, an oxidizing step at 1×10^{-6} mbar O$_2$ pressure for 10 min at 800 K, and a final annealing/oxygen desorption step at 1100 K for 10 min. The IL doses were calibrated with a quartz crystal microbalance in close proximity to the sample in the preparation chamber. After

IL deposition on the sample at 157 K, the sample was then quickly transferred within 4–8 min to the pre-cooled AFM/STM sample stage in the analysis chamber at 110 K for the measurements. After annealing at selected temperatures for a given time in the analysis chamber, STM images were then again recorded at 110 K using a tungsten tip in constant current mode. The images were processed with Gwyddion software and moderate filtering. The processing included background subtraction and 2D FFT filtering. For a consistent scaling, some images were cut in Gwyddion and/or CorelDraw software, which was used to prepare the figures.

ARXPS measurements were done in a different two-chamber XPS system equipped with a non-monochromated Al Kα X-ray source (SPECS XR 50, 1486.6 eV, 240 W) and a hemispherical electron analyzer (VG SCIENTA R3000); for details see ref. 33. The Pt(111) surface was cleaned by Ar$^+$ ion sputtering (600 eV), annealing at 1100 K for 10 min, oxidizing for 10 min at 800 K at 1×10^{-7} mbar, and a final annealing/desorption step at 1000 K for 10 seconds. For all spectra, a pass energy of 200 eV was used, yielding an overall energy resolution of ~ 1 eV. The spectra were evaluated quantitatively using CasaXPS V2.3.16Dev6. The intensity of the Pt 4f signal was obtained by numerical integration from 77.0 to 66.0 eV binding energy after subtraction of a constant background adjusted at low binding energy. This method proved to be more robust towards adsorbate-induced changes in the Pt 4f satellite structure than subtraction of a Shirley or linear background. For the IL-related S 2p, C 1s, N 1s, O 1s and F 1s regions, linear backgrounds were subtracted and the peaks were fitted with Voigt profiles (30% Lorentzian contribution). Additionally, the widths (fwhm) and some positions of the peaks were constrained (see Table S4 in the ESI†). All spectra were referenced to the Fermi edge yielding 71.2 eV for the Pt 4f$_{7/2}$ signal.
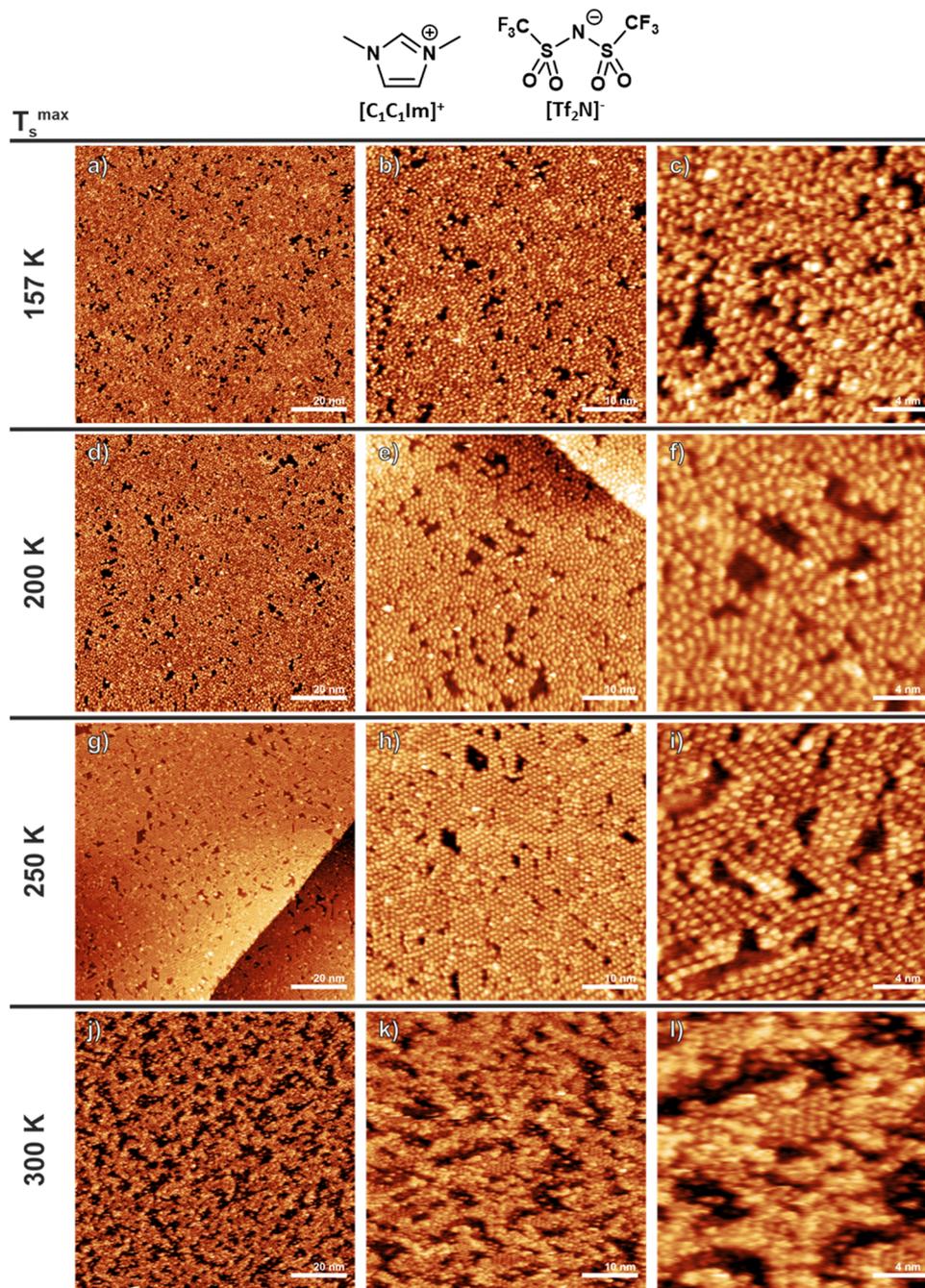
Results and discussion

Structure and growth behavior

To start with, we investigated the adsorption of [C_1C_1Im][Tf_2N] on Pt(111) at low temperature using scanning tunneling microscopy (STM). Fig. 1 shows the corresponding images of a nearly closed wetting layer (~ 0.5 ML) at different temperatures. All layers were prepared by evaporating the IL onto the Pt(111) surface in the preparation chamber, with the surface at a temperature of 157 K. The sample was then quickly transferred within a few minutes to the STM chamber and cooled to 110 K, where all STM measurements have been performed. Fig. 1 shows images recorded directly after sample transfer (with 157 K as maximum temperature), and after stepwise heating to 200, 250 and 300 K, in each case at this temperature for 10 min. For each temperature, three representative images are shown at different scales of (left) 100×100 nm^2, (middle) 50×50 nm^2, and (right) 20×20 nm^2.

Upon deposition at 157 K and subsequent measurement at 110 K, a disordered, nearly closed 2D layer is formed (Fig. 1a–c). We can identify individual protrusions, which we tentatively

27954 | *Phys. Chem. Chem. Phys.*, 2023, **25**, 27953–27966

This journal is © the Owner Societies 2023

Fig. 1 STM images of a nearly closed $[C_1C_1Im][Tf_2N]$ wetting layer ($\sim$0.5 ML; originally deposited at 157 K) on Pt(111) at different scales: (left) 100 × 100 nm^2, (middle) 50 × 50 nm^2, and (right) 10 × 10 nm^2. (a)–(c) Measured after deposition, (c)–(f) after annealing to 200 K for 10 min, (d)–(f) after annealing to 250 K for 10 min, and (j)–(l) after annealing to 300 K for 10 min. Brighter features correspond to higher elevation. All STM images were measured after cooling back to 110 K with U_{bias} = 1.2 V and I_{set} of 0.2 to 0.5 nA (for details, see Table S5 in the ESI†). At the top of the figure the chemical structure of $[C_1C_1Im][Tf_2N]$ is shown.

assign to the $[Tf_2N]^-$ anions. While this assignment is not unequivocal, it is based on the adsorption geometry derived from ARXPS (see below): The anions have a much higher elevation due to their adsorption in *cis* conformation, with the CF$_3$ groups pointing away from the surface, while the cations lie flat on the surface. Overall, the different protrusions have very similar brightness, with only a few being brighter

than the others. Annealing to 200 K for 10 min induces ordering in the adsorbed layer, which indicates an enhanced mobility of the IL ions on the surface at this temperature. In Fig. 1d–f, highly ordered regions with stripe-like or hexagonal local structure can be observed. Again, most of the protrusions have very similar brightness, and only a few are brighter than the others. Upon heating to 250 K (Fig. 1g–i), the surface order

further increases, now displaying larger regions with mostly hexagonal order and homogeneously bright protrusions. At the same time, however, the number of individual brighter features has significantly increased (best seen at the 50×50 nm^2 scale in Fig. 1h). Obviously, other processes in addition to ordering occur at this temperature, which will later be identified as the onset of decomposition of the IL (see below). Upon heating to 300 K, dramatic changes are observed (Fig. 1j–l). The ordered regions have strongly decreased in number, but can still be recognized, being indicative of intact IL on the surface. In addition, large areas show a disordered appearance with a broad variation in brightness, in particular, the number of very bright (and fuzzy) features has strongly increased. We attribute these observations to the decomposition of the IL (see below).

The appearance of the ordered regions in Fig. 1 is similar to structures that were recently observed on Au(111) by our group.[35] They are attributed to a checkerboard-like structure of intact IL, in which the cations and anions adsorb alternatingly next to each other. This type of behavior has been observed for many ILs on different metal surfaces and is governed by strong attraction of the ions towards the metal.[16]

In addition to the STM experiments, we also studied the initial growth behavior of $[C_1C_1Im][Tf_2N]$ on Pt(111) by ARXPS, after depositing increasing amounts of IL by PVD at sample temperatures of 100, 180 and 200 K, where the IL is intact (see also below). To deduce the growth mode, we analyzed the attenuation of the Pt 4f substrate signal, $I_d/I_{d=0}$, at $\theta = 0°$ (normal) and $\theta = 80°$ (grazing) emission as a function of the nominal thickness of the deposited IL film, using our previously established approach, see Fig. 2.[16] Thereby, for each deposition experiment, the mean thickness d of the film is first determined from $I_d/I_0 = \exp(-d/\lambda \cos\theta)$ for $\theta = 0°$, that is, in the bulk-sensitive geometry. Thereby, λ is the inelastic mean free path length of the Pt 4f photoelectrons within the IL (extrapolated to be 3.10 nm at 1415 eV kinetic energy[33]). With the obtained d value, we can then predict the attenuation at 80° for a two-dimensional IL layer at this thickness (for details of this approach, see ref. 16,33): the short-dashed grey lines represent ideal layer-by-layer 2D growth; deviations lying above the curve indicate a three-dimensional (3D) film morphology. For the here-studied system, the 80° data follows the prediction for ideal layer-by-layer growth up to ~1.0 ML (~0.7 nm for $[C_1C_1Im][Tf_2N]$[33]), indicating that at low coverages initially a closed wetting layer forms, where all ions are in direct contact with the metal surface in a checkerboard arrangement, which is in line with the observations by STM (see above). This 2D growth continues up to a coverage of 1 ML, which indicates that above the wetting layer, another 2D IL layer on top forms with the same thickness. Above this 1 ML coverage, the 80° data fall above the prediction for ideal layer-by-layer growth. Such a behavior has been observed before for other ILs on different metals and indicates the growth of "moderate" 3D islands on top of the initially formed 2D layers.[16] Notably, the initial 2D growth and subsequent 3D growth occurs similarly at 100, 180 and 200 K.
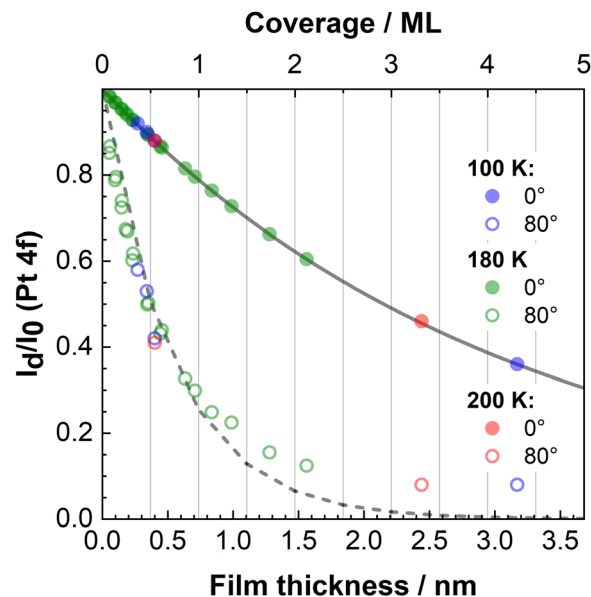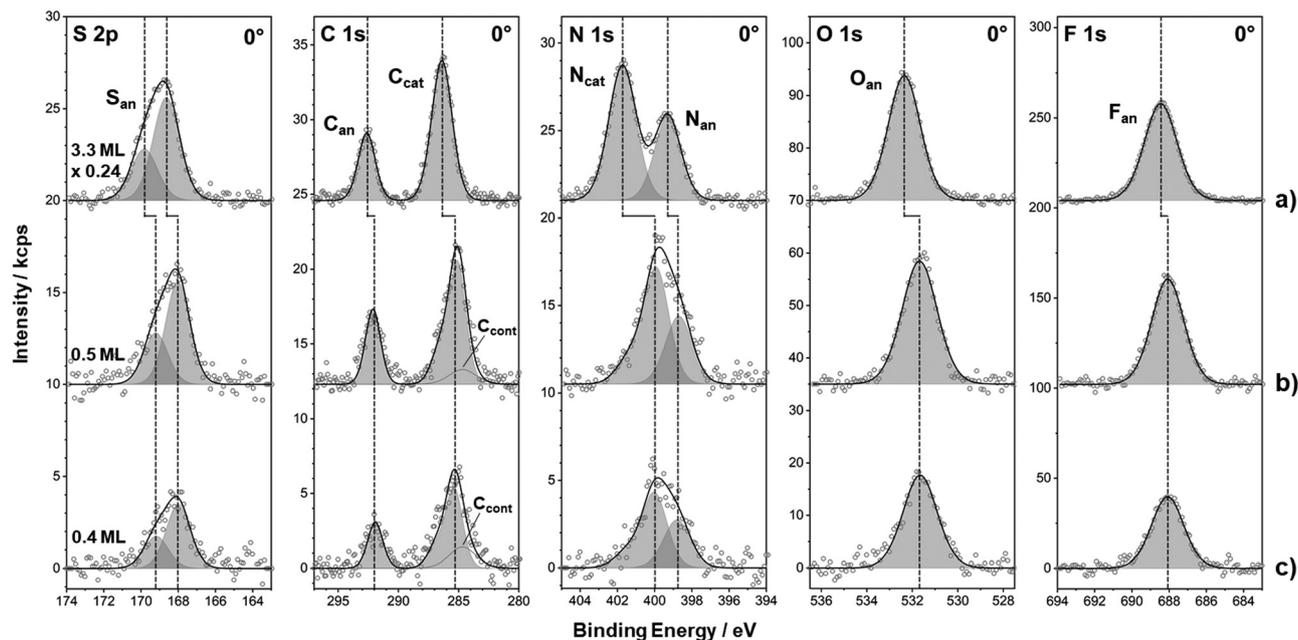

Fig. 2 Dependence of the Pt 4f substrate signal (full symbols for 0° and open symbols for 80° emission) on IL film thickness for $[C_1C_1Im][Tf_2N]$ on Pt(111) at 100, 180 and 200 K. The film thickness of each layer was calculated from the attenuation of the Pt 4f signal at 0°. The solid and dashed lines show the exponential decay expected for a uniform increase in layer thickness for emission angles of 0° and 80°, respectively,[16] based on the inelastic mean free path λ of 3.1 nm for the Pt 4f peak. Up to ~1.0 ML, very good agreement of the 80° data with the dashed lines is found, indicating the formation of a 2D layer. For larger coverages, pronounced deviations from 2D growth are observed (for details see text).

Chemical composition at low temperature

To study the interaction of the IL with the Pt(111) surface, we investigated nominal coverages of 0.4 and 0.5 ML, which are below and close to the completion of the wetting layer, respectively, by ARXPS of all relevant core levels (note that the coverages of different preparations varied from 0.47–0.52 ML for the "0.5 ML" spectra and from 0.35–0.39 ML for the "0.4 ML" spectra; for details, see Table S6, ESI†). The sub-wetting layer coverage data (0.4 ML) were measured to rule out multilayer features in the spectra; due to their better signal-to-noise ratios, the discussion will mostly focus on the 0.5 ML data in the following. For comparison, we also measured spectra of a 3.3 ML (2.4 nm) thick film, which serve as reference for the measurements of the thinner films. We start with discussing the data of the 3.3 ML (multilayer) film at 200 K, which was evaporated onto the surface at this temperature. The corresponding S 2p, C 1s, N 1s, O 1s and F 1s spectra were collected at an emission angle of 0° (normal emission) and are shown in Fig. 3a. Two of the observed signals are assigned to the $[C_1C_1Im]^+$ cation: The C_{cat} peak at 286.4 eV stems from the three carbon atoms of the imidazolium ring and the two carbon atoms of the methyl groups attached to the nitrogen atoms. The N_{cat} peak at 401.9 eV corresponds to the two nitrogen atoms in the imidazolium ring. The remaining signals are assigned to the $[Tf_2N]^-$ anion: The C_{an} peak at 292.6 eV and the F_{an} peak at 688.5 eV originate from the carbon and the fluorine atoms of the CF$_3$ group, respectively. The O_{an} peak at 532.4 eV and the

27956 | *Phys. Chem. Chem. Phys.*, 2023, **25**, 27953–27966

This journal is © the Owner Societies 2023

0.4, 0.5 & 3.3 ML [C$_1$C$_1$Im][Tf$_2$N] on Pt(111) at 200 K

Fig. 3   S 2p, C 1s, N 1s, O 1s and F 1s spectra of [C$_1$C$_1$Im][Tf$_2$N] on Pt(111). (a) 3.3 ML deposited at 200 K and measured at 200 K; (b) 0.5 ML deposited at 200 K and measured at 200 K, and (c) 0.4 ML deposited at 100 K and measured at 200 K. For a better visualization, the spectra in (a) are scaled down by a factor of 0.24. All spectra were fitted, and the corresponding results are shown as grey-shaded peaks (for peak assignment details, see text); dashed lines indicate the peak positions. In the C 1s spectra, a minor surface carbon contamination of the crystal (C$_{cont}$) was additionally taken into account for (b) and (c).

S$_{an}$ 2p$_{1/2}$/2p$_{3/2}$ doublet at 169.8/168.6 eV are assigned to the oxygen and sulfur atoms of the sulfonyl-group, respectively. Finally, the N$_{an}$ peak at 399.3 eV stems from the central imidic nitrogen. The quantitative analysis of the data is shown in Table 1, together with the nominal IL stoichiometry. The deduced atom numbers agree to the nominal values within the experimental uncertainty ($\pm$10%), which unequivocally proves that the IL evaporates as intact ion pairs and adsorbs intact at 200 K on Pt(111).

The spectra for films in the wetting layer coverage range are shown in Fig. 3b for 0.5 ML and Fig. 3c for 0.4 ML. The 0.4 ML film was deposited at 100 K and heated to 200 K while the

0.5 ML film was deposited at 200 K. Overall, the spectra for the two coverage regimes are very similar. The binding energies of the various core levels are given in Table 2, along with the corresponding values for the 3.3 ML film. To enable a better comparison, the 3.3 ML spectra in Fig. 3a were downscaled by a factor of 0.24. Apart from their lower intensity, all anion signals of the 0.4 and 0.5 ML films are overall similar as those of the 3.3 ML film. The shifts by 0.4–0.7 eV to lower binding energies of the different levels are attributed to a more efficient screening of the excited core holes in the vicinity of the platinum surface, as compared to the situation in the IL bulk.[31] For the cation signals of the 0.4 and 0.5 ML films, however, the situation is

Table 1   Quantitative composition analysis of 0.5 ML [C$_1$C$_1$Im][Tf$_2$N] films on Pt(111): after deposition at low temperatures (100 or 200 K) and subsequent heating to 200, 250 and 300 K (spectra shown in Fig. 3b and 5 bottom), and also after direct deposition at 300 K (spectra of Fig. 5 top). In addition, the results for a 0.4 ML film (deposited at 100 K) and a 3.3 ML film (deposited at 200 K) are provided (spectra of Fig. 3a and c, respectively). The numbers for anion atoms shown in brackets are re-normalized to the sum 15 for intact [Tf$_2$N]$^-$. Note that for each measurement temperature, a new layer was freshly prepared. For details, see text

	S$_{an}$	C$_{an}$	C$_{cat}$	N$_{cat}$	N$_{an}$	O$_{an}$	F$_{an}$	Σ
Nominal	2 (2)	2 (2)	5	2	1 (1)	4 (4)	6 (6)	22 (15)
3.3 ML@200 K								
Measured at 200 K	1.9	2.0	4.9	2.1	1.2	3.7	6.2	22
0.5 ML@300 K								
300 K	1.1 (1.6)	1.3 (1.9)	7.0	3.6	0.6 (0.9)	2.5 (3.7)	4.5 (6.9)	20.5 (15)
0.5 ML@100/200 K								
300 K	0.8 (1.5)	1.0 (1.9)	4.4	2.2	0.5 (1.0)	1.8 (3.4)	3.8 (7.2)	14.5 (15)
250 K	1.4 (1.6)	1.7 (2.0)	4.3	1.9	0.9 (1.0)	3.3 (3.8)	5.7 (6.6)	19.3 (15)
200 K	1.8 (1.7)	2.0 (1.9)	4.5	2.0	1.0 (1.0)	4.0 (3.9)	6.7 (6.5)	22 (15)
100 K	1.7 (1.6)	2.0 (1.9)	4.2	1.8	1.1 (1.0)	4.5 (4.2)	6.7 (6.3)	22 (15)
0.4 ML@100 K								
200 K	1.6	1.8	4.4	1.9	1.1	4.4	6.8	22

Table 2 Binding energies of the different core levels for 0.5 ML $[C_1C_1Im][Tf_2N]$ on Pt(111). The 100 K film was deposited at 100 K, the other films at 200 K; derived from the XP spectra shown in Fig. 3b and 5 (bottom). In addition, also the results for the 0.4 ML film (deposited at 100 K) and the 3.3 ML film (deposited at 200 K) in Fig. 3a and c, respectively, are provided

	S $2p_{3/2an}$ [eV]	C $1s_{an}$ [eV]	C $1s_{cat}$ [eV]	N $1s_{cat}$ [eV]	N $1s_{an}$ [eV]	O $1s_{an}$ [eV]	F $1s_{an}$ [eV]
3.3 ML							
200 K	168.6	292.6	286.4	401.9	399.3	532.4	688.5
0.5 ML							
300 K	168.1	292.2	285.1	400.1	398.9	531.7	688.2
250 K	168.1	292.1	285.1	400.0	398.8	531.7	688.2
200 K	168.0	292.1	285.1	399.9	398.7	531.7	688.1
100 K	168.3	292.2	285.4	400.0	398.8	532.0	688.2
0.4 ML							
200 K	168.0	291.9	285.4	400.0	398.8	531.7	688.1

quite different, as is evident from the peak fitting in Fig. 3b and c. The C_{cat} peak at 285.1 eV and the N_{cat} peak at 399.9 eV (for 0.5 ML) display much larger shifts towards lower binding energies, by 1.3 and 2.0 eV, respectively (the shifts for 0.4 ML are by 0.1–0.3 eV smaller). In addition, we observe a weak shoulder at higher binding energy in both regions (close to the positions of the 3.3 ML bulk film). Notably, we fitted the cation signals in the C 1s and N 1s spectra for 0.4 and 0.5 ML in Fig. 3 considering this high binding energy shoulder, which leads to a strongly asymmetric line shape. We propose that these line shapes originate from cations in the wetting layer, which are adsorbed flat on the Pt(111) surface with strong covalent bonding interactions involving charge transfer between the π-orbitals of the imidazolium and platinum. We attribute these to IL in the ordered phases observed in the STM images in Fig. 1.

Thermal evolution

The stability and thermal evolution of $[C_1C_1Im][Tf_2N]$ films on Pt(111) was studied *in situ* by temperature-programmed XPS (TPXPS). 0.4, 0.5 and 1.3 ML thick films were each prepared at 100 K and heated to 600 K with a constant heating rate of 2 K min^{-1}. Simultaneously, the Pt 4f, F 1s and C 1s regions were measured at 0°. Thereafter, the 0.5 ML sample was flash-heated to 800 K for about 1 min, and spectra were measured at 600 K. We consider the F_{an} and C_{cat} peaks as representative for the anion and cation coverage, respectively, and use them to follow the thermal evolution; notably, all other anion and cation signals were not measured for time reasons and to minimize beam damage in the TPXPS series (a detailed analysis at selected temperatures is provided below). In Fig. 4a–c, the temperature-induced intensity changes are shown for the F_{an} (violet diamonds), C_{cat} (dark grey squares; note that fitting of the C_{cat} signal with its low signal-to-noise ratio in TPXPS was simplified using only one broad peak instead of the shape described above using a main line plus high binding energy shoulder) and Pt 4f signals (light grey circles). In this type of plot, a decrease of IL-related signals indicates desorption of anion- or cation-related species from the surface, which is accompanied by an increase in the Pt 4f substrate signal due to the corresponding decrease in surface coverage.

Fig. 4a and b show that the 0.4 and 0.5 ML films behave very similar, apart from the lower signals of the former due to its lower initial coverage. Both show constant Pt 4f, C_{cat} and F_{an}
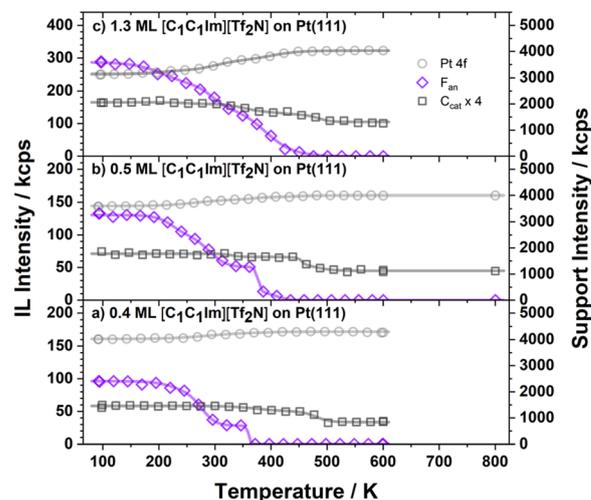
Fig. 4 Thermal evolution of the Pt 4f (light grey circles), F_{an} (violet diamonds) and C_{cat} (dark grey squares) intensities during heating of $[C_1C_1Im][Tf_2N]$ films on Pt(111): (a) 0.4 ML, (b) 0.5 ML, and (c) 1.3 ML. The IL was first deposited onto the sample at low temperature *via* PVD; thereafter, XP spectra were recorded while heating with a linear heating rate of 2 K min^{-1} up to 600 K; after a final flash heating of the 0.5 ML sample to 800 K for about 1 min, a last data set was also recorded at 600 K. The intensity scale for the Pt 4f signal is given on the right side and that of the F_{an} and C_{cat} signals on the left.

intensities between 100 and ~200 K, which indicates that the IL films stays chemically intact in this temperature window. Above 200 K, the F_{an} intensity, indicative of the adsorbed anions, continuously decreases by ~60% to reach a plateau between ~300 and ~375 K, with ~40% of the original intensity. At the same time, the C_{cat} intensity, indicative of adsorbed cations, remains constant until ~300 K, and thereafter shows a minor decrease (by less than 10%) to reach a plateau between ~375 and ~450 K. Upon further heating, the anion intensity drops rapidly to zero at ~385 K, while the cation intensity stays constant. Finally, starting at ~450 K, the cation intensity decreases by another 30%, to reach a plateau at ~475 K, with ~60% of its original intensity. In the absence of any anion signal, this signal is attributed to a residual carbon species, which is remaining at the Pt surface even up to 800 K. Simultaneously to the decrease of the IL-related signals, the Pt 4f substrate signal increases accordingly, reflecting the coverage decrease due to desorption of anion- and cation-related species.

We propose the following interpretation of these TPXPS experiments. For coverages up to the full wetting layer and temperatures below 200 K, the IL is fully intact with anions and cations in direct contact with the Pt(111) surface. Upon further heating, the IL starts to decompose above 200 K. The anion-related reaction products are volatile and leave the surface, as reflected in the decrease in F_{an} signal until a plateau is reached between $\sim$300 and $\sim$375 K, at around 40% of its original intensity. For charge neutrality reasons, we assume that a similar fraction of the cations also undergoes decomposition. In contrast to the desorbing anion decomposition products, the decomposed cation fragments remain at the surface exhibiting similar C 1s and N 1s binding energies as the intact cations. We also propose that the remaining 40% of anion and also cation signals within the plateau between $\sim$300–375 K correspond to still intact IL (see below). This scenario implies that in course of the ongoing IL decomposition, the surface becomes less and less reactive due to an increasing amount of cation-derived decomposition products. When a certain coverage of decomposition products is reached, further IL decomposition is suppressed, and still intact IL remains stable, until desorption or further decomposition occurs above 375 K. The remaining carbon signals seen at higher temperatures in Fig. 4 thus originate from the cation decomposition process.

As the film thickness might play an important role for the performance of SCILL catalysts, we also studied the thermal evolution of an IL coverage of 1.3 ML, which corresponds to a full wetting layer plus IL multilayers on top of it. The corresponding data are shown in Fig. 4c (note the changed IL intensity range as compared to Fig. 4a and b). The anion
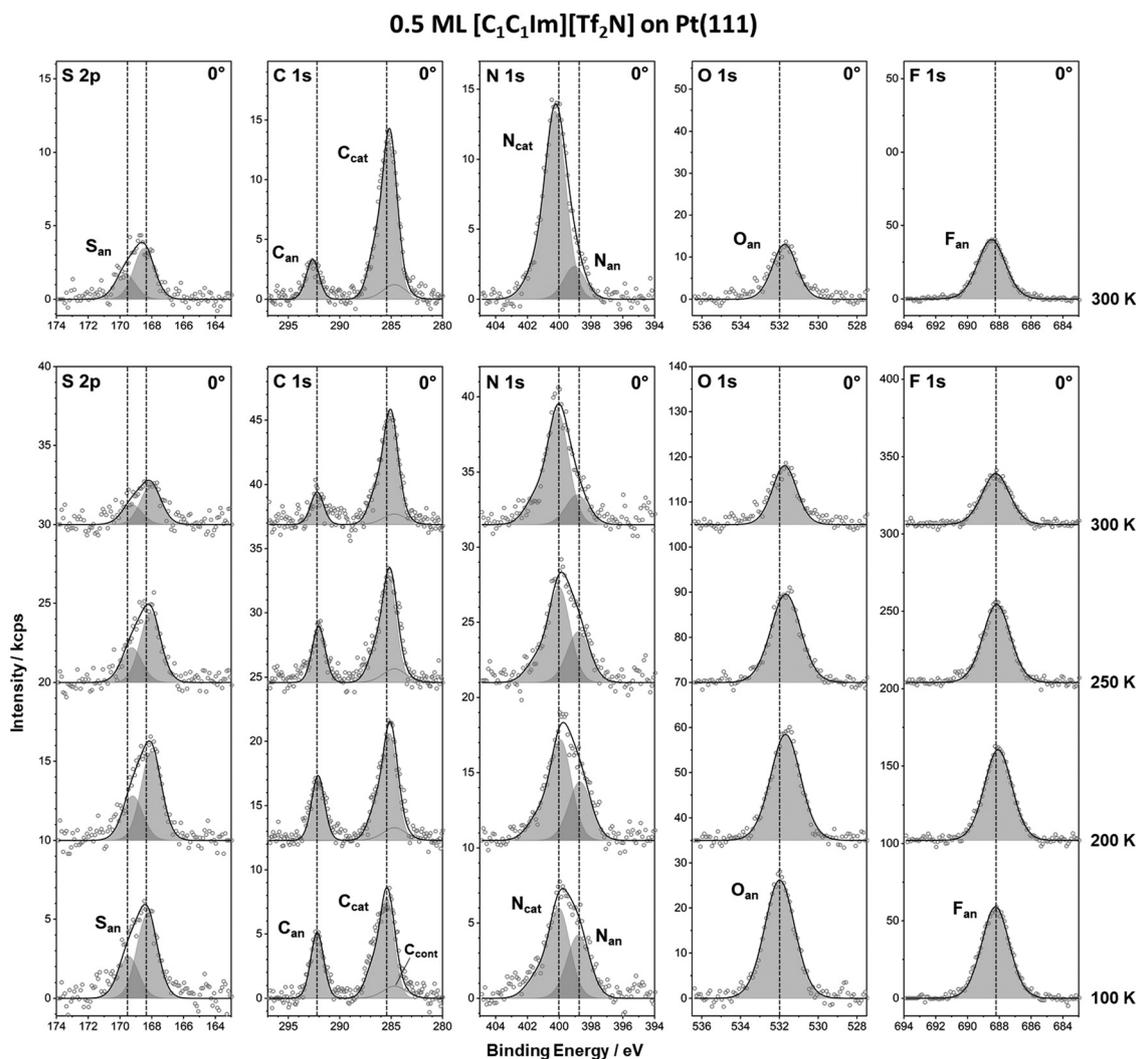
Fig. 5 S 2p, C 1s, N 1s, O 1s and F 1s spectra of [C₁C₁Im][Tf₂N] on Pt(111). (Bottom part) After low temperature deposition of 0.5 ML and heating to the denoted temperatures (the 100 K film was deposited at 100 K, the other films at 200 K); for each temperature, a new layer was freshly prepared (the exact coverages of the individual layers varied between 0.47 and 0.52 ML; see Table S6, ESI†). (Top row) IL deposition at 300 K up to a total film thickness equivalent to 0.5 ML intact IL. All spectra were fitted, and the corresponding results are shown as grey-shaded peaks. In the C 1s spectra, a small contamination of the surface (C_cont) was taken into account. The dotted lines indicate the binding energy positions of the film at 100 K. Note that the spectra for 0.5 ML at 200 K are the same as the spectra in Fig. 3b.

intensity decreases continuously starting at around ∼175 K and vanishes at ∼450 K, which is about 75 K higher than for the low coverages. The evolution of the cation intensity is similar to that of the 0.4 and 0.5 ML films. The smaller Pt 4f intensity at 100 K is due to the stronger damping by the thicker IL layer. The observed behavior can be understood considering that for the 1.3 ML film ions on top of the wetting layer are not in direct contact with the Pt(111) surface. Hence, the interface-related decomposition, desorption and surface passivation processes at the IL-metal interface likely are superimposed by additional exchange processes between multilayer (which desorbs at 345 K[16]) and wetting layer: Surface sites emptied by desorption of the anion-related decomposition products can be refilled by intact IL, which partly decomposes again and partly is stable up to 450 K, due to an increasing degree of passivation by the cation decomposition products. In line with this interpretation, the remaining carbon intensity above 500 K, which is higher for the 1.3 ML film than for the 0.5 and 0.4 ML films (note the different scale), indicates that overall more IL ions underwent decomposition upon heating.

Characterization at selected temperatures

For a more detailed characterization of the thermally induced processes, we performed isothermal measurements of all relevant IL core levels of 0.5 ML and 0.4 ML films at 100, 200, 250 and 300 K. Note that each temperature set represents a freshly prepared film on the clean Pt(111) surface to avoid accumulation of beam damage effects (individual deposition temperatures and coverage values are given in the corresponding figure captions). After deposition or after heating to the indicated temperatures, a full set of ARXP spectra was measured. The corresponding spectra along with their fits in 0° emission are shown in Fig. 5 (bottom part) and Fig. S1 (ESI†) for 0.5 ML, and Fig. S2 (ESI†) for 0.4 ML; notably, the 200 K data are the same as shown in Fig. 3. The quantitative analyses are summarized in Table 1 and Tables S1, S2 (ESI†), respectively. The more surface sensitive spectra measured at 80° (Fig. 6 and Fig. S1, S2, ESI†) will be discussed later. Since the 0.5 and 0.4 ML films behave qualitatively the same at all temperatures, we focus the following discussion on the 0.5 ML films due to the better signal-to-noise ratios.

The 100 and 200 K spectra for the 0.5 ML films in Fig. 5 look very similar. The overall intensities and the resulting atom numbers (Table 1) agree with each other and with the nominal values within the experimental uncertainty of ±15% (the somewhat larger deviation for the S_{an} signal is due to some uncertainties in the background subtraction). The good agreement for all core levels again confirms intact IL in contact with Pt(111) up to 200 K, in line with the TPXPS experiments discussed in Fig. 4. The small peak shifts towards lower binding energy (−0.3 eV) at 200 K, mainly seen for the S 2p and O 1s anion peaks, are likely due to a reorganization of the ions at the surface: Due to the low mobility at temperatures well below 200 K, the IL adsorbs in different adsorption geometries, as witnessed by the disorder observed in the STM images (see Fig. 1a–c, deposited at 157 K and measured at 110 K). At 200 K,

the increased thermal energy allows for obtaining the energetically more favorable adsorption geometry, that is, a checkerboard-type arrangement, with the SO_2 groups of the anion preferentially pointing downwards, which is typically observed for other metal surfaces.[18,19,21,25–27,31,33,40–47] This orientation at 200 K is also confirmed by our 80° spectra (see below). The close proximity of the SO_2 groups to the metal surface allows for a better core hole screening of the S and O atoms of the anion, leading to the observed small shifts.[31] The C_{cat} and N_{cat} peaks also show minor changes concerning binding energy and intensity (note that the C 1s and N 1s peaks of the cation are fitted with the same shoulder as used in Fig. 3, yielding the same asymmetric line shapes), reflecting some reorganization of the cations as well at 200 K.

For higher temperatures, the TPXPS experiments in Fig. 4 indicated desorption and/or decomposition of the IL, while in STM we observed an increased formation of disordered regions. Indeed, also the XP spectra at 250 K in Fig. 5 display a decrease of the anion signals by ∼15%, compared to the 200 K spectra, while the intensities and binding energy positions of the cation signals remain virtually unchanged. At 300 K, the anion signals have decreased by ∼50% as compared to 200 K, while the cation signals still remain unaffected. For both anion and cation signals, the binding energies undergo minor shifts (up to 0.2 eV) to higher binding energy. The loss of anions from the surface as compared to 100 K is also reflected from the atomic numbers in Table 1 (note that the total atom number, given in the last column Σ has been adapted to account for the desorbing anion fragments). The observed behavior indicates that up to 300 K ∼50% of the anion-related species desorb from the surface while the amount of cation-related species remains more or less constant up to 300 K. At this temperature, the STM data shown in Fig. 1 reveal the formation of the disordered phase at the expense of the ordered islands.

In the following, we provide evidence that the remaining S_{an}, C_{an}, N_{an}, O_{an} and F_{an} signals at 250 and 300 K originate from intact IL on the surface, and that all anion-related decomposition products have desorbed. In Table 1 all anion values given in brackets are re-normalized to the sum of atoms of $\Sigma = 15$ for an intact $[Tf_2N]^-$ anion. The deviations of the measured values from the stoichiometry are quite small (<20%), which is in line with intact anions present at the surface at 250 and 300 K. Thus, the isothermal measurements strongly support our above-proposed behavior upon linear heating, namely that at 300 K a significant fraction of the adsorbed IL decomposes, and the undecomposed IL fraction remains on the surface. The anion-related decomposition products are volatile above 200 K and desorb from the surface while the cation-related decomposition products remain on the surface and have similar binding energy positions as the intact IL cations. This self-passivation allows for maintaining non-decomposed IL anions and cations in the wetting layer even at 300 K. The decrease of the anion signal to ∼40% in the TPXPS experiment as compared to ∼50% in the isothermal 300 K measurements is likely due to the fact that the plateau at 40% is not yet fully reached at 300 K (see Fig. 4). The STM data are also in line with this interpretation, as upon heating the ordered phase increasingly

27960 | *Phys. Chem. Chem. Phys.*, 2023, **25**, 27953–27966

This journal is © the Owner Societies 2023

converts to a disordered phase assigned to intact IL coexisting with cation-related disordered decomposition products.

To evaluate possible decomposition mechanisms of the IL, we additionally studied the thermal evolution of 0.5 ML of the trimethylated $[C_1C_1C_1Im][Tf_2N]$. The motivation for this measurement is that decomposition of the IL above 200 K could start with partial deprotonation of the imidazolium cation forming a strongly bound carbene at the Pt-surface. The proton could then react with the anions to form neutral bistriflimidic acid (Tf_2NH), which subsequently desorbs above 200 K. The additional methyl group in $[C_1C_1C_1Im][Tf_2N]$ protects the most acidic C_2 carbon atom of the cation, where deprotonation should start.[48,49] The TPXPS data in Fig. S3a (ESI†), and the isothermal XPS data in Fig. S4 (ESI†) along with the quantitative analysis in Table S3 (ESI†) show that the anion and cation signals of this IL evolve virtually identical to those of the di-methylated $[C_1C_1Im][Tf_2N]$. The unchanged thermal behavior strongly indicates that deprotonation of the C_2 carbon most likely is not the initial decomposition step for the wetting layer of $[C_1C_1Im][Tf_2N]$ on Pt(111). We refrain from further speculating on the nature of the observed decomposition process since its products are difficult to assess. The anions could decompose to volatile fragments like NH_x, SO_x and CF_x species, similar as proposed for the same IL on Cu(111).[21] Ideally, temperature programmed desorption experiments would be helpful, but are out of the scope of this work. The nature of the cation-related species also cannot be identified from the C 1s and N 1s peaks.

Orientation of the IL in the wetting layer regime

In a next step, we address the orientation of the anions and cations in the wetting layer regime. This information can be derived by comparing the spectra of all relevant core levels at 0° and 80° emission of our ARXP spectra: Thereby, a larger signal of a specific atom at 80° (as compared to 0°) indicates that this atom is located closer to the vacuum side of the ultrathin IL film, and *vice versa*, a smaller signal indicates that this atom is closer to the Pt(111) surface. In Fig. 6, the corresponding spectra of the 0.5 ML films are shown (0°: black; 80°: red); note that the 0° spectra are the same as those already shown in Fig. 5 (bottom). In addition, the fitted spectra along with the quantitative analysis are provided in Fig. S1 and Table S1 (ESI†). The corresponding data for the 0.4 ML films are shown in Fig. S2 and Table S2 (ESI†). In our analysis, we focus on the changes in intensity with emission angle of the F_{an} signal (representative of the CF_3 group of the anion), the O_{an} signal (SO_2 group of the anion) and the C_{cat} signal. The C_{an} and N_{cat} signals behave qualitatively the same as the F_{an} and C_{cat} signal, respectively. Note that the S_{an} signal has a larger uncertainty due to challenges with background subtraction. As the behavior for 0.4 ML and 0.5 ML is very similar, we concentrate discussing the behavior of the latter.

At 100 K, the F_{an} signal at 80° in Fig. 6 is significantly larger than at 0°, and the O_{an} signal significantly smaller. This behavior is also reflected in the quantitative analysis provided
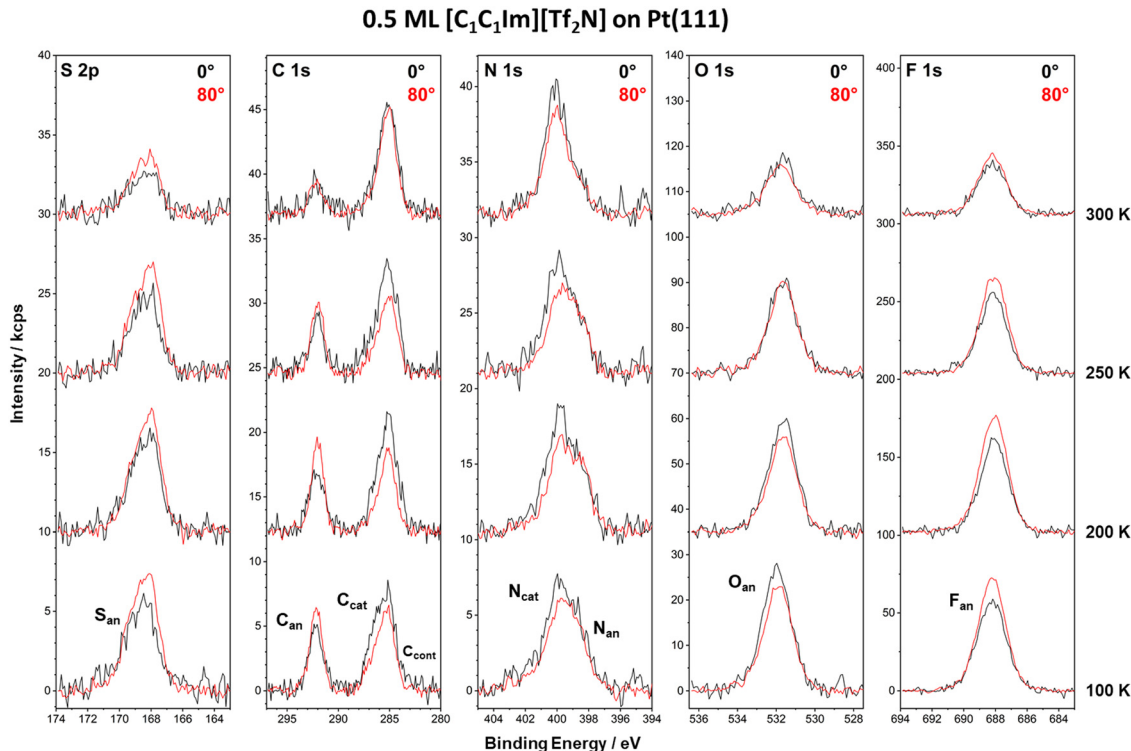
Fig. 6 S 2p, C 1s, N 1s, O 1s and F 1s spectra of 0.5 ML $[C_1C_1Im][Tf_2N]$ on Pt(111) after low temperature deposition and heating to the denoted temperatures (the 100 K film was deposited at 100 K, the other films at 200 K); for each temperature, a new layer was freshly prepared (the exact coverages of the individual layers varied between 0.46 and 0.54 ML; see Table S6, ESI†) and measured under normal (0°; black) and grazing emission (80°; red). Note that the spectra in 0° are the same as shown in Fig. 5 (bottom).

This journal is © the Owner Societies 2023

Phys. Chem. Chem. Phys., 2023, **25**, 27953–27966 | **27961**

in Table S1 (ESI†), where the atom number for F_{an} at 80° is larger than the nominal one (8.1 vs. 6) and for O_{an} lower than the nominal one (3.7 vs. 4). For the N_{an} atoms (which are in the center of the anion) no angle dependence was seen. These observations indicate that the anion is oriented with the CF_3 groups preferentially pointing towards the vacuum side and the SO_2 groups towards the metal surface. This characteristic orientation has been observed for similar systems with similar anions.[18,19,21,25–27,31,33,40–47] For the C_{cat} signal, we measure a decrease at 80° in Fig. 6, which goes along a with a lower than nominal atom number C_{cat} at 80° in Table S1 (ESI†) (3.3 vs. 5), which is in line with the cation ring lying flat in close proximity to the metal surface.

At 200 K, the F_{an} signal further increases (8.4 vs. 6, at 80°), while the O_{an} (3.4 vs. 4) and C_{cat} (3.1 vs. 5) signals further decrease. This effect is attributed to the increased mobility at this temperature, which enables the IL to obtain its optimum adsorption geometry. At 100 K, the IL has low mobility, yielding a moderate preferential orientation. At 200 K, the IL film is better equilibrated, yielding a higher, more uniform degree of orientation. This interpretation is in line with our STM results in Fig. 1, where at 200 K highly ordered IL islands are observed. Notably, the orientation effects are to some extent also reflected in the bulk sensitive 0° measurements, as it was also observed for other (sub-)wetting layer IL systems.[18,21] This effect is most prominent for the F_{an} signal at 200 K (6.7 vs. 6; see Table S1, ESI†).

At 250 and 300 K, the differences between 0 and 80° in Fig. 6 become increasingly less pronounced. We attribute this behavior to a lower degree of order, since above 200 K decomposition of the IL sets in with desorption of anion-related decomposition products (see above). The remaining IL is coadsorbed with the cation-related decomposition products, which could lead to different, less well-oriented adsorption geometries, which might particularly affect the order and the orientation of the remaining anions. Further, entropic effects (e.g. cis–trans isomerization of $[Tf_2N]^-$) also could contribute to the less pronounced orientation at the higher temperatures.

Our findings for $[C_1C_1Im][Tf_2N]$ on Pt(111) are compatible to results published by Hohner et al. for a closely related system, that is, $[C_2C_1Im][Tf_2N]$ on Pt(111).[26] The only difference of the two ILs is an ethyl group instead of a methyl group in the cation, and thus, one would expect a similar adsorption behavior (note that the authors use a different coverage definition, that is, 1 ML as full wetting layer coverage in their study, which corresponds to 0.5 ML in our study; further, they use an alternative name for $[Tf_2N]$, namely $[NTf_2]$). Hohner et al. exposed the Pt(111) surface to $[C_2C_1Im][Tf_2N]$ at 200 and 300 K, and analyzed the geometry of the $[Tf_2N]^-$ anion in the (sub-)wetting layer regime using infrared absorption spectroscopy (IRAS) at 200 and 300 K in combination with DFT calculations.[26] For both temperatures, IRAS indicates a coverage dependence of the molecular orientation in the wetting layer range. At low coverages, the $[Tf_2N]^-$ anion predominantly adsorbs with the S–N–S bonds parallel to the surface: the CF_3 groups point towards the vacuum side while the SO_2 groups point towards the metal surface in a 2–1 bonding motif, that is, one SO_2 group binds via one oxygen atom and the

other SO_2 group binds via both oxygen atoms to the metal. Interestingly, the authors rule out a 2–2 bonding motif (all oxygen atoms of both SO_2 groups point towards the metal) due to missing peaks in the IRAS spectra. We want to note, however, that a mixture of anions coadsorbed in 2–2 or 2–1 motif is still compatible with their data, in particular, since the DFT-derived adsorption energies even favor the former (2.74 eV for 2–2 vs. 2.51 eV for 2–1). Reaching wetting layer saturation, Hohner et al. proposed a change of the adsorption motif towards an upright standing species that binds only via both oxygen atoms of one SO_2 group, while the other SO_2 group is lifted from the surface (so-called 2–0 cis motif); notably, this adsorption motif is found to be not stable in their DFT calculation.[26] Independent of coverage, the $[C_2C_1Im]^+$ cations are proposed to adopt an orientation with the imidazolium ring parallel to the metal surface.

While the IRAS data by Hohner et al.[26] and our ARXPS data for wetting layers of $[C_2C_1Im][Tf_2N]$ and $[C_1C_1Im][Tf_2N]$, respectively, on Pt(111) are more or less consistent, our interpretation is, however, different: From ARXPS, we know that a $[C_1C_1Im][Tf_2N]$ wetting layer deposited at 100 K decomposes to 50–60% upon heating to 300 K, with the anion-related reaction products desorbing instantaneously and the cation-related products remaining on the surface. Thereby, the surface is partly passivated, enabling the remaining IL to still be adsorbed intact at 300 K. Notably, IRAS is not sensitive to flat-lying cations or decomposition products without a dipole moment perpendicular to the surface, due to the metal-surface selection rule.[26] Therefore, Hohner et al. did not consider any influence of the described decomposition and surface passivation process on their IRAS data.

Adsorption at 300 K

As a last step, we investigated the adsorption of $[C_1C_1Im][Tf_2N]$ on Pt(111) directly at 300 K; notably in our above-described experiments, 0.5 ML IL films were deposited at 100 or 200 K, and then further heated to 300 K. Interestingly, when deposition is done at 300 K, the dose required to reach a surface coverage of 0.5 ML (as deduced from the attenuation of the Pt 4f signal) was about twice as large as the one required at 100 K. The corresponding XP spectra at 0° in Fig. 5 (top part) can be directly compared to the spectra measured at 100 K (Fig. 5, bottom) and after annealing to 300 K (Fig. 5, bottom). The quantitative analysis is provided in Table 1. After deposition at 100 K, the atomic numbers were in line with the nominal values (within ±10%), reflecting the adsorption of the intact IL. After heating to 300 K, the cation intensities in Fig. 5 (bottom) were unchanged, but those of the anion decreased to ~50% due to IL decomposition and desorption of the anion-related products. After direct deposition at 300 K, the situation is quite different: The cation signals in Fig. 5 (top) are much larger than after annealing to 300 K, while the anion signals have an intensity between those obtained after deposition at 100 K and after annealing to 300 K, indicative of massive IL decomposition. These observations can be understood based on our explanation proposed above: during deposition at 300 K, a fraction of the anions decomposes and instantaneously desorbs opening free space for further adsorption of IL, where again
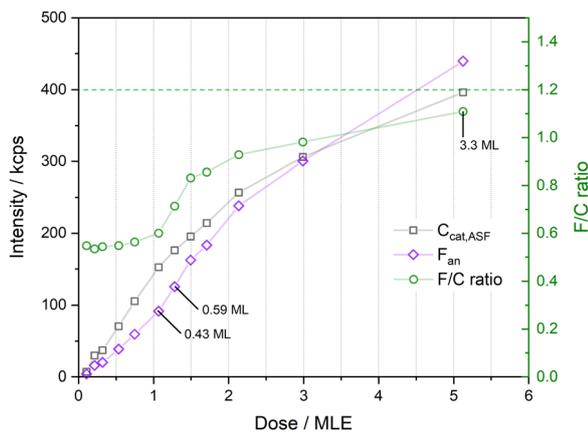
27962 | Phys. Chem. Chem. Phys., 2023, 25, 27953–27966

This journal is © the Owner Societies 2023

Fig. 7 Intensity of the C_{cat} signal (grey) and F_{an} signal (violet) of $[C_1C_1Im][Tf_2N]$ on Pt(111), as a function of IL dose at 300 K. Both signals are corrected by the respective atomic sensitivity factors to allow for a direct quantitative comparison of their absolute intensities. In addition, also the $F_{an}:C_{cat}$ ratio is depicted (green; scale on the right side); the dashed horizontal line indicates the nominal ratio $F_{an}:C_{cat} = 6:5 = 1.2$, reflecting the six F_{an} atoms and five C_{cat} atoms of the intact IL.

anions partly decompose, with the products desorbing. Hence, cation-related species accumulate at the expense of anions until one fully closed wetting layer is formed (=0.5 ML of decomposition products plus IL). This explains the higher dose required to reach an equivalent 0.5 ML coverage at 300 K as compared to 100 K. Due to the higher dose, more intact IL can adsorb on the surface, which explains the larger anion signal for deposition at 300 K as compared to annealing to 300 K. The quantification of the anion signals in Table 1 reveals atom numbers close to the nominal values, indicating that the remaining IL is indeed intact.

To study the behavior from sub-wetting layer coverages up to the multilayer range at room temperature, we sequentially deposited at 300 K increasing amounts of $[C_1C_1Im][Tf_2N]$ on Pt(111) and measured the Pt 4f, F_{an} and C_{cat} signals each time. In Fig. 7, the F_{an} (violet diamonds) and C_{cat} (grey squares) signal intensities are plotted against the dose in MLE; thereby 1 MLE (monolayer equivalent) is the dose required to obtain a coverage of 1 ML at 100 K. Additionally, the $F_{an}:C_{cat}$ ratio for each dose (green circles) is shown, along with the nominal ratio $F_{an}:C_{cat} = 6:5 = 1.2$ of an intact IL (green dashed horizontal line). At low doses, the $F_{an}:C_{cat}$ ratio is ~0.55, which is less than half of the nominal value, which reflects the desorption of anion-related decomposition products. This ratio remains more or less constant up to doses ~1 MLE, where the surface at 300 K is actually covered only by 0.43 ML of decomposition products plus IL, which is close to the nominal coverage of one closed layer of 0.5 ML. At higher doses, the F_{an} signal increases strongly and the $F_{an}:C_{cat}$ ratio finally approaches the nominal value of 1.2. This indicates that after forming one closed layer composed of decomposition products plus IL, the Pt(111) surface is passivated and IL can co-adsorb intact without decomposition. At high doses, the slopes of the C_{cat} and also the F_{an} curves decrease, due to self-damping in the thin IL layer.

At this point, we come back to the study by Hohner et al. for $[C_2C_1Im][Tf_2N]$ on Pt(111).[26] The authors also observed that a

considerably higher IL dose was required to reach a closed first layer (wetting layer) at 300 K as compared to deposition at 200 K. Moreover, they assumed a change in anion orientation in this layer when reaching the full wetting layer coverage at 300 K. As mentioned above, Hohner et al. did not consider any decomposition effects at this temperature. They attributed the required higher dose to a smaller sticking coefficient, and the change in orientation to lateral interactions within the IL layer and not to the coadsorption of decomposition products. We therefore propose that their interpretation should be reconsidered. Moreover, our ARXPS results might also explain the discrepancy concerning the upright adsorption geometry of the IL for the full wetting layer with the DFT calculations in the study by Hohner et al.[26]

Conclusions

We have investigated the adsorption and thermal evolution of the ionic liquid $[C_1C_1Im][Tf_2N]$ on Pt(111) in the temperature range from 100 to 800 K. Information about adsorbate structure, growth behavior, and chemical composition as function of temperature was obtained from angle-resolved X-ray photoelectron spectroscopy and scanning tunneling microscopy. Our measurements concentrated on the coverage required to achieve a fully covered surface, the so-called wetting layer. 0.5 and 0.4 ML of the IL were deposited at low temperature (100 or 200 K), followed by heating to 250/300 K, or directly at 300 K.

Upon IL deposition and adsorption at 100/157 K, initially an intact, disordered layer is formed. At 200 K, long range order, as deduced from STM, and molecular orientation, as deduced from ARXPS, become more pronounced; the IL still is fully intact, adsorbed in a checkerboard-type structure with anions and cations in direct contact with the Pt(111) surface. Upon heating to 250 K, the surface order further increases, but simultaneously indications of IL decomposition are seen in both STM and XPS. Further heating to 300 K leads to enhanced IL decomposition of 50–60% of the IL. The anion-related reaction products are volatile and leave the surface, as reflected in the decrease in F_{an} signal until a plateau is reached between ~300 and ~375 K, at around 40% of its original intensity. For charge neutrality reasons, we assume that a similar fraction of the cations also undergoes decomposition. In contrast to the desorbing anion fragments, the cation fragments remain at the surface exhibiting similar C 1s and N 1s binding energies as the intact cations. We propose that the remaining 40% of anion and also cation signals within the plateau between ~300–375 K correspond to still intact IL. This scenario implies that in the course of the ongoing IL decomposition, the surface becomes less and less reactive due to an increasing amount of cation-derived decomposition products. When a certain coverage of decomposition products is reached, further IL decomposition is suppressed, and still intact IL remains stable until desorption or further decomposition occurs above 375 K. The remaining carbon signals seen at higher temperatures originate from the cation decomposition process.

Comparing our results to an earlier IRAS study for the closely related system $[C_2C_1Im][Tf_2N]$ adsorbed on Pt(111),[26]

This journal is © the Owner Societies 2023

Phys. Chem. Chem. Phys., 2023, **25**, 27953–27966 | **27963**

we found similar orientation effects for the intact IL in the wetting layer; however, Hohner *et al.* were not aware of decomposition effects occurring at room temperature due to the reduced spectral sensitivity with respect to the cations and remaining decomposition products. In any case, we propose that the observed decomposition and resulting partial surface passivation might play an important role to understand observed selectivity effects in SCILL catalysis.

Our findings show the complexity of the processes occurring at the IL/metal interface of our model SCILL system, which are relevant for real SCILL systems in general. Strong covalent interactions of the IL with the platinum surface – as witnessed by the pronounced chemical shifts found for the imidazolium cation signals – modify catalytic sites and hence, might promote or suppress their catalytic behavior. In course of a surface passivation, very reactive but unselective sites that even lead to the decomposition of the IL are likely blocked by strongly adsorbed decomposition products (originating from the imidazolium cations in our case) and thus, could increase the selectivity of the catalytic process. Moreover, these IL-derived decomposition products might also be beneficial in the context of platinum-based fuel cell catalysis using ionic liquid coatings.[28] An understanding of these types of phenomena at the IL/metal interface on the molecular level might indeed help to understand the catalytic behavior of real systems on the macroscopic scale.

Author contributions

Conceptualization, S. M., F. M., H.-P. S.; methodology, S. M., T. T., L. W., C. C. F. (XPS), A. G., M. M., S. J., R. A., A. B. (STM); validation, S. M., A. G., A. B., F. M., H.-P. S.; formal analysis, S. M., A. G.; investigation, S. M., T. T., L. W., C. C. F. (XPS), A. G., M. M., S. J., R. A. (STM); resources, H.-P. S.; data curation, S. M. (XPS), A. G. (STM); writing – original draft preparation, S. M., A. G.; writing – review and editing, S. M., F. M., H.-P. S.; visualization, S. M., A. G.; supervision, F. M., H.-P. S.; project administration, F. M., H.-P. S.; funding acquisition, H.-P. S., C. C. F. All authors have read and agreed to the published version of the manuscript.

Conflicts of interest

There are no conflicts to declare.

Acknowledgements

References

1 C. R. Catlow, M. Davidson, C. Hardacre and G. J. Hutchings, Catalysis making the world a better place, *Philos. Trans. R. Soc., A*, 2016, **374**(2061), 20150089.

2 J. Hagen, *Industrial Catalysis: A Pratical Approach*, Wiley-VCH Verlag GmbH & Co. KgaA, 2005.

3 N. V. Plechkova and K. R. Seddon, Applications of ionic liquids in the chemical industry, *Chem. Soc. Rev.*, 2008, **37**(1), 123–150.

4 K. R. Seddon, A taste of the future, *Nat. Mater.*, 2003, **2**(6), 363–365.

5 A. J. Greer, J. Jacquemin and C. Hardacre, Industrial Applications of Ionic Liquids, *Molecules*, 2020, **25**(21), 5207.

6 U. Kernchen, B. Etzold, W. Korth and A. Jess, Solid Catalyst with Ionic Liquid Layer (SCILL) – A New Concept to Improve Selectivity Illustrated by Hydrogenation of Cyclooctadiene, *Chem. Eng. Technol.*, 2007, **30**(8), 985–994.

7 W. Korth and A. Jess, Solid Catalysts with Ionic Liquid Layer (SCILL), in *Supported Ionic Liquids*, ed. F. Rasmus, A. Riisager and M. Haumann, Wiley-VCH Verlag GmbH & Co. KGaA, 2014, pp. 279–306.

8 H.-P. Steinrück and P. Wasserscheid, Ionic Liquids in Catalysis, *Catal. Lett.*, 2015, **145**(1), 380–397.

9 O. Bartlewicz, I. Dąbek, A. Szymańska and H. Maciejewski, Heterogeneous Catalysis with the Participation of Ionic Liquids, *Catalysts*, 2020, **10**(11), 1227.

10 M. Sobota, M. Happel, M. Amende, N. Paape, P. Wasserscheid, M. Laurin and J. Libuda, Ligand Effects in SCILL Model Systems: Site-Specific Interactions with Pt and Pd Nanoparticles, *Adv. Mater.*, 2011, **23**(22–23), 2617–2621.

11 J. Arras, E. Paki, C. Roth, J. Radnik, M. Lucas and P. Claus, How a Supported Metal Is Influenced by an Ionic Liquid: In-Depth Characterization of SCILL-Type Palladium Catalysts and Their Hydrogen Adsorption, *J. Phys. Chem. C*, 2010, **114**(23), 10520–10526.

12 L. Naicker, M. Schörner, D. Kremitzl, H. B. Friedrich, M. Haumann and P. Wasserscheid, Influencing the Product Distribution in Citral Hydrogenation Using Ionic Liquid Modified Cu Catalysts, *ChemCatChem*, 2022, **14**(19), e202200388.

13 T. Barth, W. Korth and A. Jess, Selectivity-Enhancing Effect of a SCILL Catalyst in Butadiene Hydrogenation, *Chem. Eng. Technol.*, 2017, **40**(2), 395–404.

14 N. Szesni, R. Fischer, A. Hagemeyer, F. Großmann, J. Boyer, H. C. Hou, D. M. Lowe, C. Lugmair, M. Sun and M. Urbancic, *Catalyst composition for selective hydrogenation with improved characteristics*, European Patent Application, EP2583751B1, 2013.

15 Clariant OleMax® 260: New acetylene selective hydrogenation catalyst starts strong at Dow, https://www.clariant.com/en/Corporate/News/2018/05/Clariant-Olemax-260-new-acetylene-selective-hydrogenation-catalyst-starts-strong-at-DOW (accessed 09.05.2023).

16 M. Lexow, F. Maier and H.-P. Steinrück, Ultrathin ionic liquid films on metal surfaces: adsorption, growth, stability and exchange phenomena, *Adv. Phys.: X*, 2020, **5**(1), 1761266.

17 H.-P. Steinrück, Recent developments in the study of ionic liquid interfaces using X-ray photoelectron spectroscopy and potential future directions, *Phys. Chem. Chem. Phys.*, 2012, **14**(15), 5010–5029.

27964 | *Phys. Chem. Chem. Phys.*, 2023, **25**, 27953–27966

This journal is © the Owner Societies 2023

18 S. Massicot, T. Sasaki, M. Lexow, S. Shin, F. Maier, S. Kuwabata and H.-P. Steinrück, Adsorption, Wetting, Growth, and Thermal Stability of the Protic Ionic Liquid Diethylmethylammonium Trifluoromethanesulfonate on Ag(111) and Au(111), Langmuir, 2021, 37(39), 11552–11560.

19 B. Uhl, H. Huang, D. Alwast, F. Buchner and R. J. Behm, Interaction of ionic liquids with noble metal surfaces: structure formation and stability of [OMIM][TFSA] and [EMIM][TFSA] on Au(111) and Ag(111), Phys. Chem. Chem. Phys., 2015, 17(37), 23816–23832.

20 M. Meusel, A. Gezmis, S. Jaekel, M. Lexow, A. Bayer, F. Maier and H.-P. Steinrück, Time- and Temperature-Dependent Growth Behavior of Ionic Liquids on Au(111) Studied by Atomic Force Microscopy in Ultrahigh Vacuum, J. Phys. Chem. C, 2021, 125(37), 20439–20449.

21 R. Adhikari, S. Massicot, L. Fromm, T. Talwar, A. Gezmis, M. Meusel, A. Bayer, S. Jaekel, F. Maier, A. Görling and H.-P. Steinrück, Structure and Reactivity of the Ionic Liquid [C$_1$C$_1$Im][Tf$_2$N] on Cu(111), Top. Catal., 2023, DOI: 10.1007/s11244-023-01801-y.

22 B. Uhl, F. Buchner, S. Gabler, M. Bozorgchenani and R. J. Behm, Adsorption and reaction of sub-monolayer films of an ionic liquid on Cu(111), Chem. Commun., 2014, 50(62), 8601–8604.

23 T. Cremer, L. Wibmer, S. Krick Calderón, A. Deyko, F. Maier and H.-P. Steinrück, Interfaces of ionic liquids and transition metal surfaces—adsorption, growth, and thermal reactions of ultrathin [C$_1$C$_1$Im][Tf$_2$N] films on metallic and oxidised Ni(111) surfaces, Phys. Chem. Chem. Phys., 2012, 14(15), 5153–5163.

24 R. Eschenbacher, S. Trzeciak, C. Schuschke, S. Schötz, C. Hohner, D. Blaumeiser, D. Zahn, T. Retzer and J. Libuda, Thermal Stability and CO Permeability of [C$_4$C$_1$Pyr][NTf$_2$]/Pd(111) Model SCILLs: from UHV to Ambient Pressure, Top. Catal., 2023, DOI: 10.1007/s11244-023-01798-4.

25 T. Bauer, S. Mehl, O. Brummel, K. Pohako-Esko, P. Wasserscheid and J. Libuda, Ligand Effects at Ionic Liquid-Modified Interfaces: Coadsorption of [C$_2$C$_1$Im][OTf] and CO on Pd(111), J. Phys. Chem. C, 2016, 120(8), 4453–4465.

26 C. Hohner, L. Fromm, C. Schuschke, N. Taccardi, T. Xu, P. Wasserscheid, A. Görling and J. Libuda, Adsorption Motifs and Molecular Orientation at the Ionic Liquid/Noble Metal Interface: [C$_2$C$_1$Im][NTf$_2$] on Pt(111), Langmuir, 2021, 37(43), 12596–12607.

27 D. Blaumeiser, C. Schuschke, L. Fromm, N. Taccardi, S. Schötz, R. Eschenbacher, H. Bühlmeyer, T. Xu, T. Bauer, P. Wasserscheid, A. Görling and J. Libuda, CO Permeability and Wetting Behavior of Ionic Liquids on Pt(111): An IRAS and PM-IRAS Study from Ultrahigh Vacuum to Ambient Pressure, J. Phys. Chem. C, 2021, 125(28), 15301–15315.

28 A. Avid, J. L. Ochoa, Y. Huang, Y. Liu, P. Atanassov and I. V. Zenyuk, Revealing the role of ionic liquids in promoting fuel cell catalysts reactivity and durability, Nat. Commun., 2022, 13(1), 6349.

29 H. Wang, Y. Wang, C. Li, Q. Zhao and Y. Cong, Introduction of Surface Modifiers on the Pt-Based Electrocatalysts to Promote the Oxygen Reduction Reaction Process, Nanomaterials, 2023, 13(9), 1544.

30 T. Sasaki, R. Izumi, T. Tsuda and S. Kuwabata, Innovative Approach for Preparing a CNT-Supported Pt Nanoparticle Functional Electrocatalyst Using Protic Ionic Liquids, ACS Appl. Energy Mater., 2021, 4(7), 7298–7308.

31 T. Cremer, M. Stark, A. Deyko, H.-P. Steinrück and F. Maier, Liquid/Solid Interface of Ultrathin Ionic Liquid Films: [C$_1$C$_1$Im][Tf$_2$N] and [C$_8$C$_1$Im][Tf$_2$N] on Au(111), Langmuir, 2011, 27(7), 3662–3671.

32 F. Rietzler, J. Nagengast, H.-P. Steinrück and F. Maier, Interface of Ionic Liquids and Carbon: Ultrathin [C$_1$C$_1$Im][Tf$_2$N] Films on Graphite and Graphene, J. Phys. Chem. C, 2015, 119(50), 28068–28076.

33 M. Lexow, T. Talwar, B. S. J. Heller, B. May, R. G. Bhuin, F. Maier and H.-P. Steinrück, Time-dependent changes in the growth of ultrathin ionic liquid films on Ag(111), Phys. Chem. Chem. Phys., 2018, 20(18), 12929–12938.

34 M. Meusel, M. Lexow, A. Gezmis, A. Bayer, F. Maier and H.-P. Steinrück, Growth of Multilayers of Ionic Liquids on Au(111) Investigated by Atomic Force Microscopy in Ultrahigh Vacuum, Langmuir, 2020, 36(45), 13670–13681.

35 M. Meusel, M. Lexow, A. Gezmis, S. Schötz, M. Wagner, A. Bayer, F. Maier and H.-P. Steinrück, Atomic Force and Scanning Tunneling Microscopy of Ordered Ionic Liquid Wetting Layers from 110 K up to Room Temperature, ACS Nano, 2020, 14(7), 9000–9010.

36 K. R. J. Lovelock, C. Kolbeck, T. Cremer, N. Paape, P. S. Schulz, P. Wasserscheid, F. Maier and H.-P. Steinrück, Influence of Different Substituents on the Surface Composition of Ionic Liquids Studied Using ARXPS, J. Phys. Chem. B, 2009, 113(9), 2854–2864.

37 S. F. Miller, H. B. Friedrich and C. W. Holzapfel, The Effects of SCILL Catalyst Modification on the Competitive Hydrogenation of 1-Octyne and 1,7-Octadiene versus 1-Octene, ChemCatChem, 2012, 4(9), 1337–1344.

38 M. T. Heinze, J. C. Zill, J. Matysik, W. D. Einicke, R. Gläser and A. Stark, Solid–ionic liquid interfaces: pore filling revisited, Phys. Chem. Chem. Phys., 2014, 16(44), 24359–24372.

39 V. Hoffmann, G. Pulletikurthi, T. Carstens, A. Lahiri, A. Borodin, M. Schammer, B. Horstmann, A. Latz and F. Endres, Influence of a silver salt on the nanostructure of a Au(111)/ionic liquid interface: an atomic force microscopy study and theoretical concepts, Phys. Chem. Chem. Phys., 2018, 20(7), 4760–4771.

40 M. Lexow, B. S. J. Heller, F. Maier and H.-P. Steinrück, Anion Exchange at the Liquid/Solid Interface of Ultrathin Ionic Liquid Films on Ag(111), ChemPhysChem, 2018, 19(22), 2978–2984.

41 S. Schernich, D. Kostyshyn, V. Wagner, N. Taccardi, M. Laurin, P. Wasserscheid and J. Libuda, Interactions Between the Room-Temperature Ionic Liquid [C$_2$C$_1$Im][OTf] and Pd(111), Well-Ordered Al$_2$O$_3$, and Supported Pd Model Catalysts from IR Spectroscopy, J. Phys. Chem. C, 2014, 118(6), 3188–3193.

42 S. Schernich, V. Wagner, N. Taccardi, P. Wasserscheid, M. Laurin and J. Libuda, Interface Controls Spontaneous Crystallization in Thin Films of the Ionic Liquid [C$_2$C$_1$Im][OTf]

This journal is © the Owner Societies 2023

Phys. Chem. Chem. Phys., 2023, 25, 27953–27966 | 27965

on Atomically Clean Pd(111), *Langmuir*, 2014, **30**(23), 6846–6851.

43 S. Mehl, T. Bauer, O. Brummel, K. Pohako-Esko, P. Schulz, P. Wasserscheid and J. Libuda, Ionic-Liquid-Modified Hybrid Materials Prepared by Physical Vapor Codeposition: Cobalt and Cobalt Oxide Nanoparticles in [C_1C_2Im][OTf] Monitored by In Situ IR Spectroscopy, *Langmuir*, 2016, **32**(34), 8613–8622.

44 C. Schuschke, L. Fromm, J. Träg, C. Stumm, C. Hohner, R. Eschenbacher, S. Grau, D. Zahn, A. Görling, T. Bauer and J. Libuda, A Molecular View of the Ionic Liquid Catalyst Interface of SCILLs: Coverage-Dependent Adsorption Motifs of [C_4C_1Pyr][NTf_2] on Pd Single Crystals and Nanoparticles, *J. Phys. Chem. C*, 2021, **125**(24), 13264–13272.

45 B. Uhl, F. Buchner, D. Alwast, N. Wagner and R. J. Behm, Adsorption of the ionic liquid [BMP][TFSA] on Au(111) and Ag(111): substrate effects on the structure formation investigated by STM, *Beilstein J. Nanotechnol.*, 2013, **4**, 903–918.

46 B. Uhl, T. Cremer, M. Roos, F. Maier, H.-P. Steinrück and R. J. Behm, At the ionic liquid|metal interface: structure formation and temperature dependent behavior of an ionic liquid adlayer on Au(111), *Phys. Chem. Chem. Phys.*, 2013, **15**(40), 17295–17302.

47 A. B. Biedron, E. L. Garfunkel, E. W. Castner and S. Rangan, Ionic liquid ultrathin films at the surface of Cu(100) and Au(111), *J. Chem. Phys.*, 2017, **146**(5), 054704.

48 A. J. Arduengo III, R. L. Harlow and M. Kline, A stable crystalline carbene, *J. Am. Chem. Soc.*, 1991, **113**(1), 361–363.

49 S. T. Handy and M. Okello, The 2-Position of Imidazolium Ionic Liquids: Substitution and Exchange, *J. Org. Chem.*, 2005, **70**(5), 1915–1918.

27966 | *Phys. Chem. Chem. Phys.*, 2023, **25**, 27953–27966

This journal is © the Owner Societies 2023